



Facile microwave hydrothermal synthesis of zinc oxide one-dimensional nanostructure with three-dimensional morphology

Jianfeng Huang^{a,b,*}, Changkui Xia^a, Liyun Cao^a, Xierong Zeng^b

^a School of Materials Science and Engineering, Shaanxi University of Science and Technology, Xi'an, Shaanxi 710021, PR China

^b Shenzhen Key Laboratory of Special Functional Materials, Shenzhen, Guangdong 518060, PR China

ARTICLE INFO

Article history:

Received 14 January 2008

Received in revised form 7 May 2008

Accepted 17 May 2008

Keywords:

Semiconductors

Zinc oxide

Diffraction

Electron microscopy

Optical properties

ABSTRACT

A facile microwave hydrothermal (M-H) solution route employing the reaction of $\text{Zn}(\text{NO}_3)_2 \cdot 6\text{H}_2\text{O}$ and NaOH under hydrothermal conditions has been demonstrated to successfully synthesize a single-crystal zinc oxide (ZnO) one-dimensional nanostructure (ODNS) with a novel three-dimensional (3D) morphology. The microwave plays an important role and is necessary for the synthesis of ZnO with the complex nanostructure. The formation mechanism of this complex nanostructure is proposed. A red shift of the absorption edge of nano-ZnO is also observed. The absence of metal catalyst, template or surfactant in this method avoids the subsequent complicated workup for the removal of the residual additives. Furthermore, a substantial reduction in the reaction time as well as the reaction temperature is observed compared with the hydrothermal process.

© 2008 Elsevier B.V. All rights reserved.

1. Introduction

The synthesis of inorganic nanocrystals is currently an active field of research in modern materials chemistry due to their wide application in catalysis, optoelectronics, microelectronics, magnetics, and biology [1–5]. Furthermore, the special attention in nanoscience and nanotechnology has been pointed toward the fabrication of materials with uniform complex structures [6–10].

Zinc oxide nanostructures have been fabricated as one-dimensional nanostructures (ODNS) and proven versatility and compatibility in numerous applications. ZnO ODNS were synthesized in the form of nanorods, nanowires, nanotubes, nanobelts, nanocombs, nanosprings, nanorings, nanobows, nanopropellers, etc. [11–14]. The wide interest in ZnO has resulted from the following fundamental characteristic features with potential applications in electronic, structural and bio-materials [12]:

- Direct band gap semiconductor (3.37 eV).
- Large excitation binding energy (60 meV).
- Near UV emission and transparent conductivity.

- Piezoelectric property resulting from its non-centrosymmetric structure.
- Bio-safe and bio-compatible.

Up to now, a number of synthetic approaches have been developed to prepare various types of ZnO ODNS using different surfactants, polymers, or templates for control of the sizes, dimensions, and morphologies of these materials. For instance, solution-based synthesis [15–21], vapor phase growth [22–31] and template-assisted synthesis [32,33]. However, the introduction of metal catalyst, surfactants, or templates into the reaction system involves a complicated process, introduces heterogeneous impurities in the products, and increases the production cost, which may restrict the wide development of research and applications. Therefore, developing a facile and metal catalyst-, surfactant- or template-free method is still of great significance [34–38], which avoids the subsequent complicated workup for the removal of the metal catalyst, template or surfactant.

Ivanov et al. [39] demonstrated a methodological approach for utilizing microwave heating during the hydrothermal process to obtain highly dispersed ZnO crystals with high photocatalytic activity. However, the employed process involves in two steps and whether the morphology of as-prepared ZnO powders can be controlled by simply adjusting the process conditions was not illustrated. Peiró et al. [40,41] prepared ZnO films with complete substrate coverage with ZnO nanorods mainly oriented perpendicularly to the substrate by a modification of the chemical bath deposition (CBD) procedure in which crystal growth is activated

* Corresponding author at: School of Materials Science and Engineering, Shaanxi University of Science and Technology, Xi'an, Shaanxi 710021, PR China. Tel.: +86 29 86168803; fax: +86 29 86168803.

E-mail address: huangjf@sust.edu.cn (J. Huang).

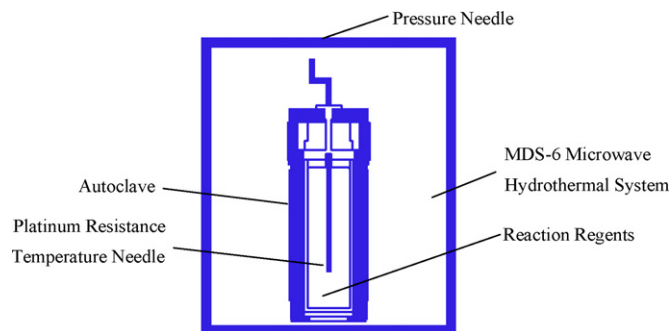


Fig. 1. Schematic diagram of preparation of ZnO nanostructure by a microwave hydrothermal process in a MDS-6 microwave hydrothermal system.

using microwave (MW) radiation. This MW-CBD technique was also used to deposit TiO₂ thin films [42–44]. However, this method produces films in an open atmosphere, not a closed system as will be demonstrated below. In the present work, we report a microwave hydrothermal (M-H) approach to prepare single-crystal ZnO ODNS with novel 3D morphology under mild conditions without the addition of any metal catalyst, surfactant or template.

2. Experimental

ZnO nanostructure was prepared by an M-H process. All of the raw materials were analytical reagent and used as-received without further purification. In a typical synthesis process, first, 15.6024 g Zn(NO₃)₂·6H₂O (1.6 mol L⁻¹) was dissolved in 32 mL deionized water to obtain Zn²⁺ solution. Secondly, 4.0960 g NaOH (3.2 mol L⁻¹) was added into the above solution with stirring at room temperature to get colloid solution. Then the solution was transferred into a 46 mL Teflon-lined autoclave and treated at a selected temperature (e.g. 413 K) for specific time (e.g. 20 min) under temperature-controlled mode or at a selected pressure (e.g. 3.0 MPa) for specific time (e.g. 20 min) under pressure-controlled mode in a MDS-6 microwave hydrothermal system (Fig. 1). The MDS-6 microwave hydrothermal system, which is manufactured by Shanghai Sineo Microwave Chemistry Technology Co. Ltd., China, can be operated under two different control modes, i.e. the temperature-controlled mode (TCM) and the pressure-controlled mode (PCM). The temperature-controlled mode maintains constant temperature while the pressure-controlled mode maintains constant pressure. The system uses non-pulsed microwave to heat the samples continuously and the microwave power is adjusted by automatic frequency conversion with the variation of temperature/pressure. The maximum microwave power is 1000 W and can be controlled continuously at four different power ranges, i.e. 0–400 W, 0–600 W, 0–800 W and 0–1000 W, according to the selected temperature/pressure.

After that the reaction was terminated and cooled to room temperature. Then the as-prepared white precipitate was collected by filtration and purified by washing with deionized water and absolute ethyl alcohol or isopropyl alcohol several times. Finally, the white precipitate was dried at 355 K in a drying cabinet with air-blasting for 2 h and the sample was obtained. The aim of the treatment at 355 K for 2 h is to remove any residual impurities, such as deionized water and absolute ethyl alcohol or isopropyl alcohol. The TG–DSC curve of nanoscale ZnO [45] shows that there is almost no mass loss during the experiment temperature range from 298 K to 1200 K and no phase transformation during the experiment temperature range from 298 K to 1773 K. This indicates that the treatment at 355 K for 2 h may not affect the sample. We conducted the experiment for different reaction times at the range

of 10–60 min. What is more, we also conducted the experiment for different [Zn²⁺] (0.2–2.0 mol L⁻¹), hydrothermal temperatures (373–473 K, under TCM), hydrothermal pressures (0.5–4.0 MPa, under PCM), and filling ratios (50–80%). We also conducted the control experiments without microwave radiation, i.e. at the same hydrothermal conditions but without microwave.

The product was characterized via X-ray powder diffraction (XRD), field-emission scanning electron microscope (FE-SEM), high-resolution transmission electron microscope (HRTEM), and UV/Vis/NIR Spectrophotometer. The XRD pattern was performed on a D/MAX-2200PC X-ray diffractometer with Cu K α radiation ($\lambda = 0.15406$ nm) and a scanning rate of 8° min⁻¹ (Rigaku, Japan). SEM images were taken on a JSM-7000F field-emission scanning electron microscope equipped with an energy-dispersive spectrometer (JEOL, Japan). HRTEM images were taken on a JEM-3010 high-resolution transmission electron microscope (JEOL, Japan). UV–vis spectra were obtained on a Lambda 950 spectrophotometer (PerkinElmer, USA). The sample was ground up lightly with agate mortar and pestle before XRD and FE-SEM characterization. The sample for TEM was prepared by dropping a diluted suspension of the sample powders onto a standard carbon-coated (20–30 nm) Formvar film on a copper grid (230 mesh). The sample for UV–vis spectra was also ground up lightly with agate mortar and pestle. The Lambda 950 spectrophotometer uses the universal reflectance accessory with a snap-in integrating sphere to measure the optical absorption. The snap-in integrating sphere can capture diffuse and specular reflectance and is available in 60 mm and 150 mm, with 8° reflectance and center mount capability. The universal reflectance accessory with dual Si and InGaAs detectors is used for automated, precise and reproducible angle adjustments and resulting high-sensitivity, absolute reflectance measurements.

3. Results and discussion

3.1. Structure and morphology

The typical XRD patterns of the ZnO nanostructure are shown in Fig. 2. All of the diffraction peaks can be readily indexed as hexagonal ZnO with lattice constants of $a = 3.249$ Å and $c = 5.206$ Å, which are consistent with the values in the standard card (JCPDS

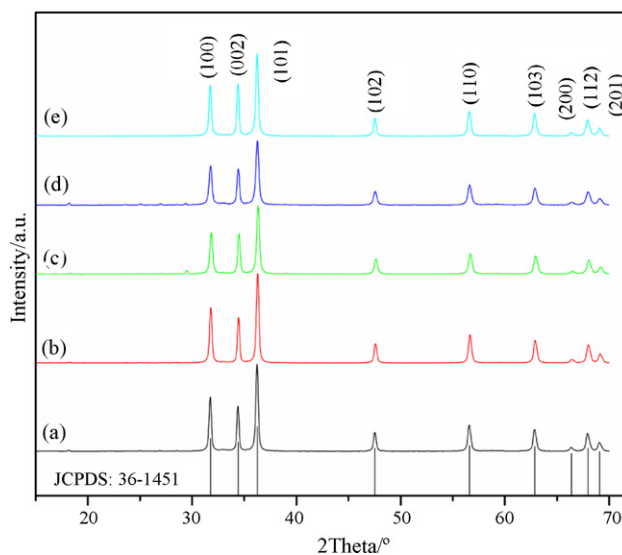


Fig. 2. XRD patterns of the as-prepared nanocrystals of ZnO nanorods (a), nanowires (b), nanorhuster vanes (c), nanodandelions (d), and nanospindles (e).

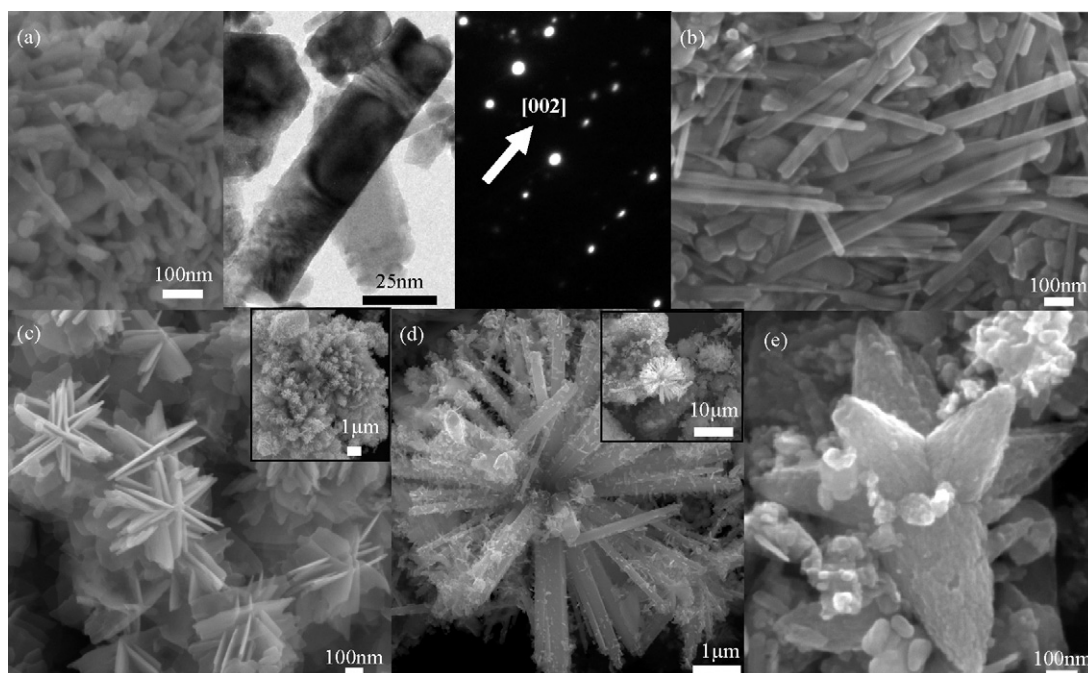


Fig. 3. FE-SEM images of the ZnO nanocrystals with different morphologies: nanorods (a, temperature = 413 K, $[Zn^{2+}] = 1.6 \text{ mol L}^{-1}$, filling ratio = 70%, time = 20 min, middle: HRTEM image and right: selected area electron diffraction (SEAD) pattern), nanowires (b, temperature = 453 K, $[Zn^{2+}] = 1.6 \text{ mol L}^{-1}$, filling ratio = 70%, time = 20 min), nanotruster vanes (c, temperature = 393 K, $[Zn^{2+}] = 1.6 \text{ mol L}^{-1}$, filling ratio = 70%, time = 20 min), nanodandelions (d, temperature = 373 K, $[Zn^{2+}] = 1.6 \text{ mol L}^{-1}$, filling ratio = 70%, time = 20 min) and radial nanospindles (e, pressure = 3.0 MPa, $[Zn^{2+}] = 0.8 \text{ mol L}^{-1}$, filling ratio = 70%, time = 20 min).

No. 36-1451). No diffraction peaks from any other impurities were detected. The strong and sharp diffraction peaks indicate that the product is crystallized.

The morphology and microstructure details of the as-prepared ZnO nanocrystals were investigated with FE-SEM. Fig. 3 shows the typical SEM images of ZnO nanostructure with different morphologies. Summary of experimental conditions and the morphology of different ZnO nanostructures are shown in Table 1. The SEM image clearly demonstrates that the majority of the crystals have a uniform nanostructure. A small portion of nanoparticles can also be observed. These nanoparticles are the intermediate products between the initial nanoparticles and the final nanostructures. The nanorods are hexagonal prisms with a typical diameter $\sim 30 \text{ nm}$ and length $\sim 100 \text{ nm}$ (Fig. 3(a)). Although there is not any dominance of the (002) peak of the diffractograms provided in Fig. 1, the peak intensities of all the peaks are remarkably enhanced compared to that obtained in control experiment. Moreover, the HRTEM image and SEAD pattern of the sample conforms the hypothesis; see Fig. 3(a) middle and right. The nanowires are hexagonal shafts with a typical diameter ranging from 10 nm to 30 nm and the length ranging from hundreds of nanometers to several micrometers (Fig. 3(b)). The nanotruster vanes are thin slices with a typical thickness and width of the slices $\sim 10 \text{ nm}$ and $\sim 400 \text{ nm}$, respectively (Fig. 3(c), inset is the low-magnification FE-SEM image). The nanodandelions are radial hexagonal prisms with a typical diameter of the petals about $10 \mu\text{m}$ (Fig. 3(d), inset is the low-magnification FE-SEM image). The most interesting case arises from the nanos-

tructure of nanospindles. They grew in three-dimensional spaces in such a pattern that several spindles grew from the same center and joined each other with the same angle in a single plane, while the rest two ones just grew along the normal directions of the plane (Fig. 3(e)). The Debye–Scherrer equation $d = K\lambda/B \cos \theta$, where d is the crystallite size, K a constant, λ the wavelength of the Cu $K\alpha$ radiation and B is the line width of the XRD peak, was used in order to determine the crystallite sizes. And the sizes calculated by Debye–Scherrer formula are consistent with the results of the FE-SEM and HRTEM.

3.2. Effect of the microwave and possible growth mechanism

The M-H process is an innovation of the conventional hydrothermal technology by introducing microwave into the reaction vessels to produce nanostructured materials more quickly [46]. The advantage of the application of microwave to the synthesis of nanomaterials is the significant reduction in fabrication time. It may be attributed to the microwave offers a kinetic process different from other methods (such as conventional hydrothermal or microemulsion) and can promise a very short reaction time and relatively stable reaction conditions.

With the assistance of microwave irradiation, the product was obtained only after 20 min reaction time under both temperature-controlled mode and pressure-controlled mode, while the prolongation of the reaction time has not remarkable influences on the final product.

Table 1
Summary of experimental conditions and the morphology of different ZnO nanostructures

Sample	Control mode	Temperature (K)	Pressure (MPa)	Time (min)	$[Zn^{2+}]$ (mol L^{-1})	Filling ratio (%)	Morphology	Crystal dimension
a	TCM	413	–	20	1.6	70	Rod	1D
b	TCM	453	–	20	1.6	70	Wire	1D
c	TCM	393	–	20	1.6	70	Thruster vane	2D
d	TCM	373	–	20	1.6	70	Dandelion	Quasi-1D
e	PCM	–	3.0	20	0.8	70	Spindle	3D

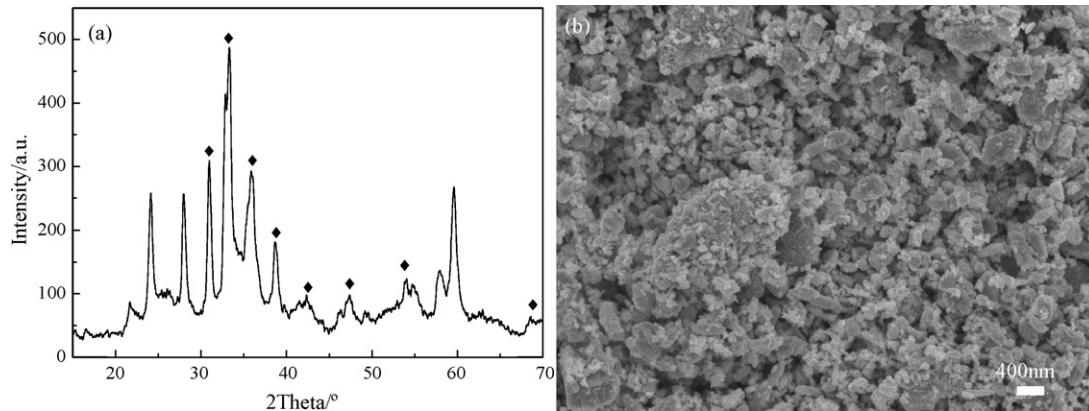


Fig. 4. XRD pattern (a) and FE-SEM image (b) of the sample obtained at the same hydrothermal conditions but without microwave irradiation compared to Fig. 3(a). The rhombuses indicate the peaks corresponding to ZnO.

Microwave heating offers many advantages over conventional autoclave heating, including rapid heating to crystallization temperature, homogeneous nucleation, and fast supersaturation by the rapid dissolution of precipitated hydroxides, which leads to lower crystallization temperatures and shorter crystallization times [47]. Such behavior leads to many unique properties in the hydrothermal solution and has been used extensively to generate novel materials with unusual properties. In the current case, the microwave may accelerate the hydrolysis of $\text{Zn}(\text{NO}_3)_2 \cdot 6\text{H}_2\text{O}$, which is presumably helpful to the nucleation and growth of ZnO nanocrystals. The experimental phenomena support the above hypothesis.

Furthermore, the rapid heating to hydrothermal temperature or pressure can accelerate solid particles to high velocities, leading to interparticle collisions and effective fusion at the point of collision. It is suggested that the microwave causes fusion of the adjacent particles and attachment of primary particles on the outer layers of the ZnO nanostructures, which are the intermediate products between the initial nanoparticles and final nanostructures. In this work, microwave plays an important role and is found to be necessary for the synthesis of ZnO with the complex 3D morphology. Fig. 4 shows the XRD pattern and FE-SEM image of the sample obtained at the same hydrothermal conditions compared to Fig. 3(a) but without microwave irradiation. The intensity and shape of the diffraction peaks in Fig. 4(a) reveal that the sample is not perfectly crystallized. Some peaks attributable to unknown impurity are observed. The SEM image (Fig. 4(b)) of the as-prepared ZnO crystals shows an irregular morphology, which is consistent with the XRD results.

Microwave appears to be particularly effective as a means of inducing nucleation and may affect the crystallization, which is responsible for the formation of final complex 3D ZnO single crystals.

In a word, the role of microwave is not only to accelerate the reaction between the raw materials but also to lead to the growth and crystallization of ZnO with complex 3D morphology.

Fig. 5 shows a condensed illustration of our strategies in the morphology control of ZnO nanostructures. First, ZnO nuclei generally evolve into nanorods by preferential *c*-axis ([002] direction) oriented 1D growth. Second, nanorods can be converted into nanowires by a multiple nanorods growth along the [002] direction and simultaneous local attachment of the polar (0001) surfaces or nanospindles by an increase in diameter and local dissolution. Third, multiple nanorods grow from center results in nanodandelions. Fourth, when the crystal growth along the [002] direction is suppressed, nanoslices can be obtained due to quasi 1D growth. Finally, when multiple nanoslices grow fur-

ther, nanotruster vanes can be formed by self-assembled growth. Take the morphology evolution of nanorods as an example: when the experiment conditions are hydrothermal temperature = 413 K, $[\text{Zn}^{2+}] = 1/2[\text{OH}^-] = 1.6 \text{ mol L}^{-1}$, filling ratio = 70%, and reaction time = 20 min, the ZnO nuclei first come into being by the inducing of the microwave irradiation; then the obtained nuclei evolve into primary ZnO nanoparticles (Fig. 6(a)). With the ongoing of the reaction, the newly generated nuclei attach to the previous

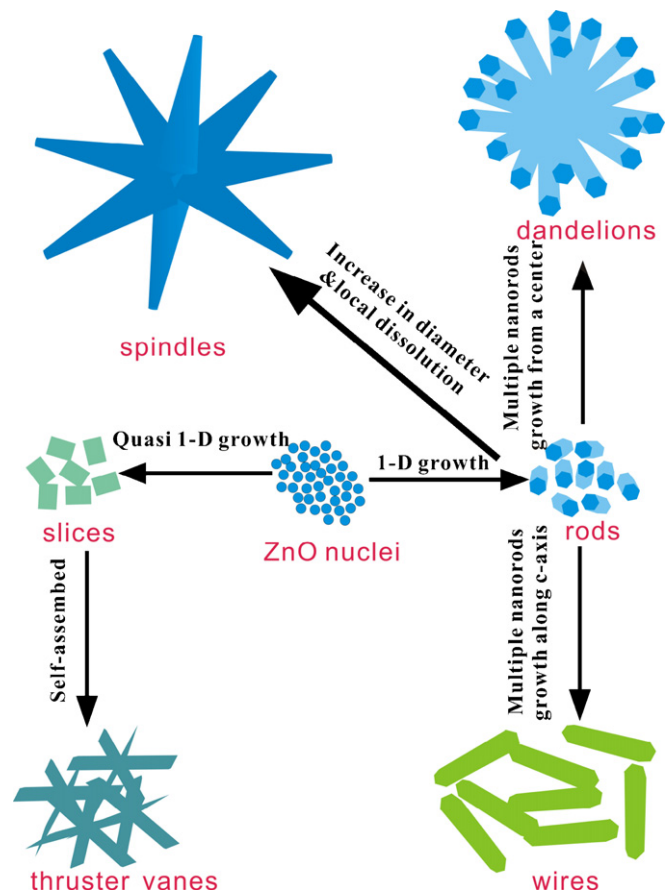


Fig. 5. Schematic of the shape-controlled synthesis of ZnO nanorods, nanowires, nanotruster vanes, nanodandelions and radial nanospindles via a microwave hydrothermal route.

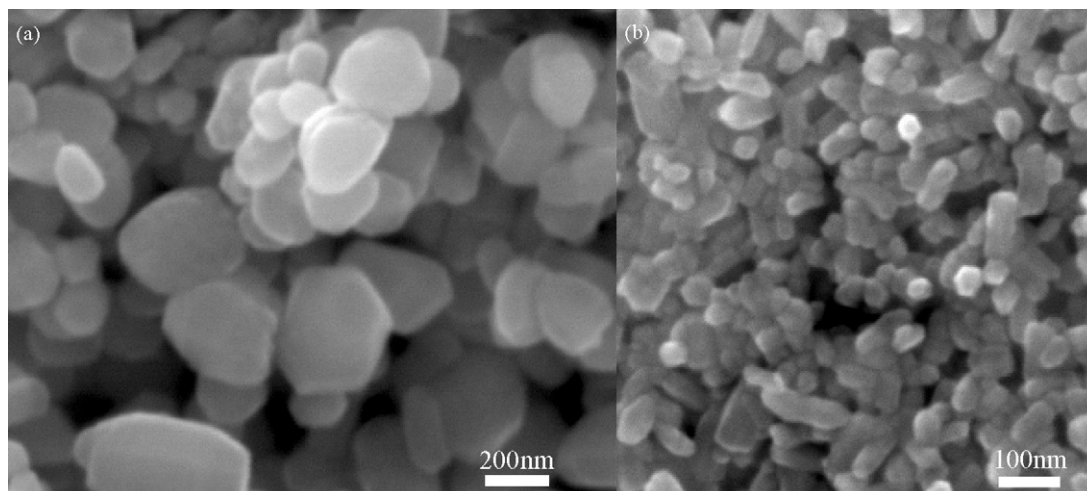
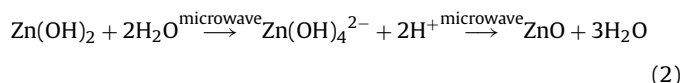


Fig. 6. FE-SEM images of nanorods at different morphology evolution stages (temperature = 413 K, $[Zn^{2+}] = 1.6 \text{ mol L}^{-1}$, filling ratio = 70%, time = 20 min).

obtained ZnO nanoparticles and lead to the further growth to the nanorods along *c*-axis (Fig. 6(b)). Finally, the hexagonal nanorods are obtained (Fig. 3(a)).

In our research, zinc cations and hydroxide anions are provided by hydration of zinc nitrate hexahydrate and NaOH, respectively. Here, zinc cations are known to readily react with hydroxide anions to form stable $Zn(OH)_4^{2-}$ complexes, which act as the growth unit of ZnO nanostructures [48,49]. Therefore, the M-H growth mechanism of ZnO nanostructures was considered as follows:



That is to say that zinc hydroxide dissolves into soluble zinc complexes, which deposit as zinc oxide under the microwave irradiation.

The employing of the microwave irradiation will accelerate the hydrolysis process, leading to the formation of the small primary ZnO nanoparticles. With the ongoing of the reaction, the primary nanoparticles further grow to the nanorod or nanoslice, and the freshly formed nanoparticles will spontaneously “land” on the as-formed rod or slice and then undergo further growth to nanowire or another slice, forming a complex structure. These processes could be related to a proposed mechanism of the so-called “orientated attachment” by Penn and Banfield [50] and Banfield et al. [51]. In this mechanism, the larger particles are grown from small primary nanoparticles through an orientated attachment process, in which the adjacent nanoparticles are self-assembled by sharing a common crystallographic orientation and docking of these particles at a planar interface. Small particles may aggregate in an oriented fashion to produce a larger single crystal, or they may aggregate randomly and reorient, recrystallize, or undergo phase transformations to produce larger single crystals. This type of growth mode could lead to the formation of faceted particles or anisotropic growth if there is sufficient difference in the surface energies of different crystallographic faces. In our case, according to the experimental results, the former seems to be more reasonable. Therefore, it is believed that the microwave hydrothermal formation of complex ZnO nanostructures undergoes three steps in sequence: (1) microwave-induced hydrolysis of $Zn(NO_3)_2$, which leads to the formation of primary ZnO nanoparticles, (2) microwave-induced fusion of these primary ZnO nanoparticles accompanying the oriented growth to form the

rod-like or slice-like structure, and (3) a further growth and crystallization process, giving rise to the formation of the 3D morphology product. Although the exact formation mechanism for this complex nanostructure is not yet exactly clear, it is believed that the growth of the complex nanostructures is not catalyst-assisted or template-directed or surfactant-modified, because the only material sources used in our synthesis are pure $Zn(NO_3)_2$ and NaOH.

3.3. Optical properties

The typical optical absorption spectra of the as-prepared samples respectively under temperature-controlled mode and pressure-controlled mode are presented in Fig. 7(a) and (c). All the cases show a strong absorption in the ultraviolet spectrum. ZnO is a direct band gap semiconductor, and therefore its absorption coefficient is related to the excitation energy ($E_{exc} = h\nu$) by $(\alpha h\nu)^2 = \text{const} - (h\nu - E_g)$, where E_g is the band gap energy [52]. To obtain the absorption onset, $(\alpha h\nu)^2$ was plotted versus energy $h\nu$ (Fig. 7(b) and (d)). And the absorption onsets obtained in Fig. 7(b) and (d) indicate that they all at the range of 3.25–3.27 eV.

Extrapolation of the linear part until its intersection with the $h\nu$ axis gives the values of E_g . From Fig. 7(b), E_g values are 3.258 eV for temperature-controlled mode and 3.264 eV for pressure-controlled mode respectively, both of them showing a red shift compared to the band gap for bulk ZnO (3.37 eV). Theoretically, a generally received opinion is that the ubiquitous blue shift of the absorption edge of nanocrystals is the result of the quantum size effect owing to the downsized crystals. But simultaneously a red shift of the absorption edge of nanocrystals may arise from an increase of the internal stress of the nanocrystals due to the decrease of the grain sizes to nanometer scale [53]. The increase of this compression stress may result in the change of the energy band structure, the overlap of the electron wave function, and finally the narrowing of band gap and energy-level width. It thus makes the optical absorption and the absorption edge induced by the electron transition from lower level to upper level or semiconductor electron transition from valence band to conduction shift to long wavelength side. Based on the discussion above, the red-shift factor in excess of blue-shift factor may be responsible for the red shift of the absorption edge of ZnO. Theories [54,55] have been established and developed to estimate the band gap of thin films [56–61], single crystals [62–65], quantum wells [66], and composites [67]. But the proposed procedures are either too complicated or quite rigorous. Zhao [68] has introduced a simple and exercisable method

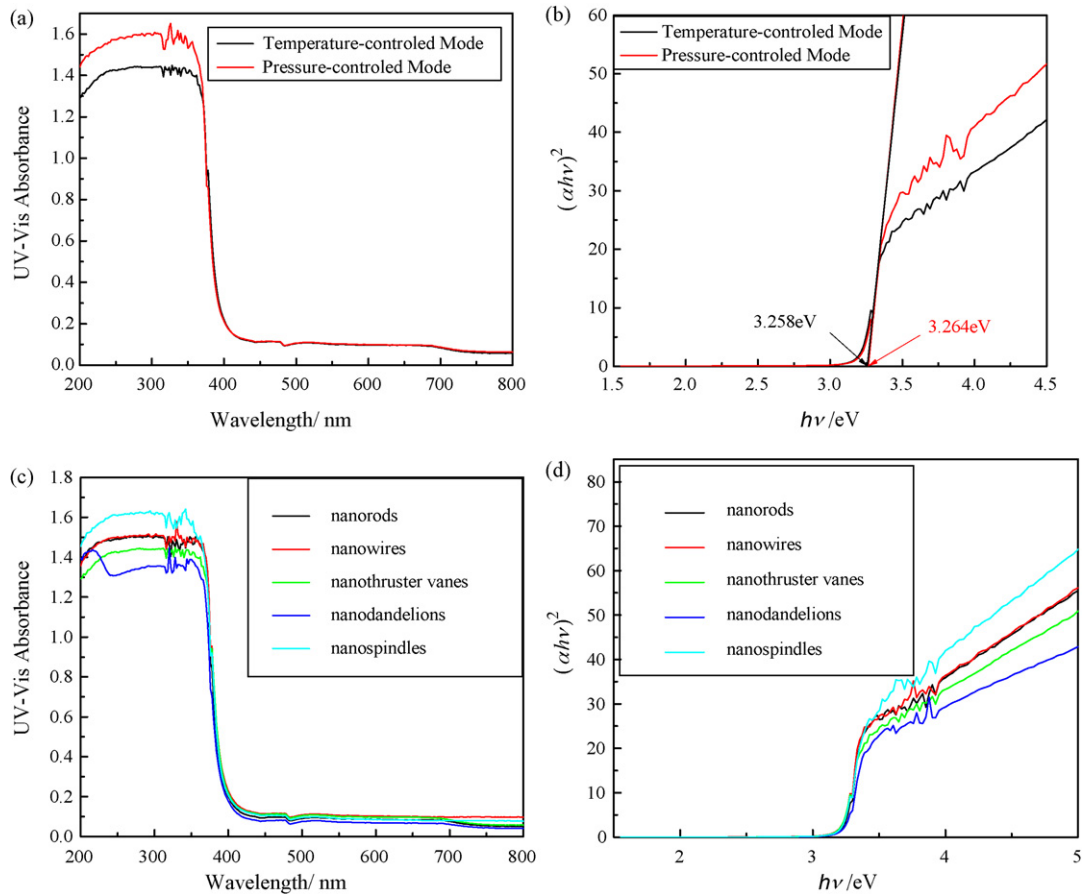


Fig. 7. (a) UV-vis absorption spectra of the as-prepared samples; (b) $(\alpha h\nu)^2$ vs. $h\nu$ plot for determining absorption onset of the as-prepared samples; (c) UV-vis absorption spectra; (d) $(\alpha h\nu)^2$ vs. $h\nu$ plot for determining absorption onset of the as-prepared samples corresponding to Fig. 3.

Table 2
Macro-stress and micro-stress of as-prepared ZnO nanocrystallites

Sample	Macro-stress, σ_{macro} (MPa)	Micro-stress, σ_{micro} (MPa)	Band gap, E_g (eV)
a	220.243	0.147	3.261
b	397.810	0.282	3.258
c	825.982	0.177	3.250
d	100.481	0.255	3.272
e	220.243	0.139	3.264

to measure the internal stress, including both the macro-stress and micro-stress, using X-ray diffractometer technique. The macro-stress and micro-stress of as-prepared ZnO nanocrystals calculated by this method are listed in Table 2. It is remarkable to note that the macro-stress is dominant, and the micro-stress is very small and can almost be eliminated. The data are fitted by polynomial fit as follows:

$$E_g = 3.2773 - 7.06041 \times 10^{-5} \sigma_{\text{macro}} + 4.58475 \times 10^{-8} \sigma_{\text{macro}}^2 \quad (3)$$

where E_g is the band gap of the samples, and σ_{macro} the macro-stress of the samples.

The internal stress, mainly the macro-stress, may arise from the decrease of the grain sizes to nanometer scale and the resultant local disorder or mismatch of crystals. Perhaps, it could be explained as the short-range disorder of the crystals that synthesized by the M-H process, in which the “orientated attachment”, as proposed above, leads to the primary ZnO nanoparticles quickly

“land” on the pre-formed rod or slice, resulting in the local disorder of the crystals. Thus, the inevitable internal stress occurs.

4. Conclusions

In summary, a facile, quick, environmentally benign M-H route to the synthesis of 3D, novel, various ZnO morphologies with single crystal structure in the absence of any metal catalyst, template or surfactant additives in a MDS-6 microwave hydrothermal system has been demonstrated. The experimental results indicate that the microwave plays the key role in the formation of the complex structure. The formation and evolution of ZnO with 3D morphology was investigated, and a possible mechanism was proposed to explain its formation. The red shift of the absorption edge of ZnO was observed and a possible origin was also proposed. The synthesis route is a process with sample maneuverability and good reproducibility and may be feasible to develop into the scale-up production. This unique complex 3D morphology may be a promising candidate for both fundamental research and functional applications and we also expect that this M-H technique can be readily adopted in realizing other forms of various nanostructured materials.

Acknowledgments

This work was supported by Program for New Century Excellent Talents in University of Ministry of Education of China (NCET-06-0893), and Foundation of Shenzhen Key Laboratory of Special Functional Materials (0701).

References

- [1] K.V. Narayana, S.K. Masthan, V.V. Rao, P.K. Rao, *J. Chem. Res. Synop.* 9 (1997) 328–329.
- [2] J.Y. Sun, S.K. Yong, K.P. Sang-Hee, *Appl. Phys. Lett.* 78 (2001) 721–723.
- [3] B.I. Lazoryak, O.V. Baryshnikova, S.Y. Stefanovich, A.P. Malakho, V.A. Morozov, A.A. Belik, I.A. Leonidov, O.N. Leonidova, G.V. Tendeloo, *Chem. Mater.* 15 (2003) 3003–3010.
- [4] S.F. Wuister, I. Swart, F. van Driel, S.G. Hickey, C.d.M. Donegá, *Nano Lett.* 3 (2003) 503–507.
- [5] M. Felix, C. Christina, C. Frank, *Angew. Chem. Int. Ed.* 43 (2004) 5954–5957.
- [6] X.X. Li, Y.J. Xiong, Z.Q. Li, Y. Xie, *Inorg. Chem.* 45 (2006) 3493–3495.
- [7] Z.H. Zhang, S.H. Liu, S.Y. Chow, M.Y. Han, *Langmuir* 22 (2006) 6335–6340.
- [8] H.G. Zhang, Q.S. Zhu, Y. Wang, *Chem. Mater.* 17 (2005) 5824–5830.
- [9] S.H. Choi, E.G. Kim, T. Hyeon, *J. Am. Chem. Soc.* 128 (2006) 2520–2521.
- [10] C.H. Lu, L.M. Qi, J.H. Yang, X.Y. Wang, D.Y. Zhang, J.L. Xie, J.M. Ma, *Adv. Mater.* 17 (2005) 2562–2567.
- [11] W.I. Park, J.S. Kim, G.-C. Yi, H.-J. Lee, *Adv. Mater.* 17 (2005) 1393–1397.
- [12] Z.L. Wang, X.Y. Kong, Y. Ding, P.X. Gao, W.L. Hughes, R. Yang, Y. Zhang, *Adv. Funct. Mater.* 14 (2004) 943–956.
- [13] G.C. Yi, C.R. Wang, W.I. Park, *Semiconduct. Sci. Technol.* 20 (2005) S22–S34.
- [14] Z. Zhu, T.L. Chen, Y. Gu, J. Warren, R.M. Osgood, *Chem. Mater.* 17 (2005) 4227–4234.
- [15] B.D. Yuhas, D.O. Zitoun, P.J. Pauzauskie, R. He, P. Yang, *Angew. Chem. Int. Ed.* 45 (2006) 420–423.
- [16] M.L. Kahn, M. Monge, V. Collière, F. Senocq, A. Maisonnat, B. Chaudret, *Adv. Funct. Mater.* 15 (2005) 458–468.
- [17] L. Vayssieres, K. Keis, S.E. Lindquist, A. Hagfeldt, *J. Phys. Chem. B* 105 (2001) 3350–3352.
- [18] J. Joo, S.G. Kwon, J.H. Yu, T. Hyeon, *Adv. Mater.* 17 (2005) 1873–1877.
- [19] L.E. Greene, M. Law, J. Goldberger, F. Kim, J.C. Johnson, Y. Zhang, R.J. Saykall, P. Yang, *Angew. Chem. Int. Ed.* 42 (2003) 3031–3034.
- [20] Y. Sun, G.M. Fuge, N.A. Fox, D.J. Riley, M.N.R. Ashfold, *Adv. Mater.* 17 (2005) 2477–2481.
- [21] J. Zhang, L.D. Sun, X.C. Jiang, C.S. Liao, C.H. Yan, *Cryst. Growth Des.* 4 (2004) 309–313.
- [22] M.H. Huang, Y. Wu, H. Feick, N. Tran, E. Weber, P. Yang, *Adv. Mater.* 13 (2001) 113–116.
- [23] M.H. Huang, S. Mao, H. Feick, H. Yan, Y. Wu, H. Kind, E. Weber, R. Russo, P. Yang, *Science* 292 (2001) 1897–1899.
- [24] Z.W. Pan, S. Dai, C.M. Rouleau, D.H. Lowndes, *Angew. Chem. Int. Ed.* 44 (2005) 274–278.
- [25] Y.J. Xing, Z.H. Xi, X.D. Zhang, J.H. Song, R.M. Wang, J. Xu, Z.Q. Xue, D.P. Yu, *Solid State Commun.* 129 (2004) 671–675.
- [26] J.H. Zhan, Y. Bando, J.Q. Hu, D. Golberg, K. Kurashima, *Small* 2 (2006) 62–65.
- [27] D. Zhao, C. Andreazza, P. Andreazza, *Phys. Status Solidi (c)* 2 (2005) 1137–1140.
- [28] Y.R. Lin, Y.K. Tseng, S.S. Yang, S.T. Wu, C.L. Hsu, S.J. Chang, *Cryst. Growth Des.* 5 (2005) 579–583.
- [29] G.Z. Shen, Y. Bando, C.J. Lee, *J. Phys. Chem. B* 109 (2005) 10578–10583.
- [30] C.H. Ye, X.S. Fang, Y.F. Hao, X.M. Teng, L.D. Zhang, *J. Phys. Chem. B* 109 (2005) 19758–19765.
- [31] S.Y. Bae, H.W. Seo, H.C. Choi, J. Park, J. Park, *J. Phys. Chem. B* 108 (2004) 12318–12326.
- [32] J.S. Jie, G.Z. Wang, Q.T. Wang, Y.M. Chen, X.H. Han, X.P. Wang, J.G. Hou, *J. Phys. Chem. B* 108 (2004) 11976–11980.
- [33] G.S. Wu, T. Xie, X.Y. Yuan, Y. Li, L. Yang, Y.H. Xiao, L.D. Zhang, *Solid State Commun.* 134 (2005) 485–489.
- [34] X.Y. Tao, X.D. Li, *Nano Lett.* 8 (2008) 505–510.
- [35] Q.F. Han, J. Lu, X.J. Yang, L.D. Lu, X. Wang, *Cryst. Growth Des.* 8 (2008) 395–398.
- [36] S.J. Guo, Y.X. Fang, S.J. Dong, E.K. Wang, *Inorg. Chem.* 46 (2007) 9537–9539.
- [37] S. Ferdov, A.M.L. Lopes, Z. Lin, R.A. Sá Ferreira, *Chem. Mater.* 19 (2007) 6025–6029.
- [38] Y.F. Zhu, D.H. Fan, W.Z. Shen, *J. Phys. Chem. C* 111 (2007) 18629–18635.
- [39] V.K. Ivanov, A.S. Shaporev, F.Yu. Sharikov, A. Ye Baranchikov, *Superlattices Microstruct.* 42 (2007) 421–424.
- [40] A.M. Peiró, C. Domingo, J. Peral, X. Domènech, E. Vigil, M.A. Hernández-Fenollosa, M. Mollar, B. Marí, J.A. Ayllón, *Thin Solid Films* 483 (2005) 79–83.
- [41] A.M. Peiró, J.A. Ayllón, J. Peral, X. Domènech, C. Domingo, *J. Cryst. Growth* 285 (2005) 6–16.
- [42] E. Vigil, J.A. Ayllón, A.M. Peiró, R. Rodríguez-Clemente, X. Domènech, J. Peral, *Langmuir* 17 (2001) 891–896.
- [43] E. Vigil, L. Saadoun, J.A. Ayllón, X. Domènech, I. Zumeta, R. Rodríguez-Clemente, *Thin Solid Films* 365 (2000) 12–18.
- [44] A.M. Peiró, E. Vigil, J. Peral, C. Domingo, X. Domènech, J.A. Ayllón, *Thin Solid Films* 411 (2002) 185–191.
- [45] Y.L. Zhang, L. Tang, *Synthetic Crystals: Growth Techniques, Properties and Applications*, 1st ed., Chemical Industry Press, Beijing, 2005, pp. 419–421 (in Chinese).
- [46] S. Komarneni, R. Roy, Q.H. Li, *Mater. Res. Bull.* 27 (1992) 1393–1405.
- [47] S. Komarneni, *Environmentally Benign Microwave Hydrothermal Processing for Synthesis of Ceramic Powders*, in: H. Yanagida, M. Yoshimura (Eds.), *Proceedings of the International Symposium on Environmental Issues of Ceramics*, Ceramic Society of Japan, Tokyo, 1995, pp. 199–206.
- [48] W.J. Li, E.W. Shi, W.Z. Zhong, Z.W. Yin, *J. Cryst. Growth* 203 (1999) 186–196.
- [49] S. Yamabi, H. Imai, *J. Mater. Chem.* 12 (2002) 3773–3778.
- [50] R.L. Penn, J.F. Banfield, *Science* 281 (1998) 969–971.
- [51] J.F. Banfield, S.A. Welch, H.Z. Zhang, T.T. Ebert, R.L. Penn, *Science* 289 (2000) 751–754.
- [52] S. Monticone, R. Tufeu, A.V. Kanaev, *J. Phys. Chem. B* 102 (1998) 2854–2862.
- [53] L.D. Zhang, J.M. Mou, *Nanomaterials and Nanostructures*, 1st ed., Science Press, Beijing, 2001 (in Chinese).
- [54] L. Brus, *J. Phys. Chem.* 90 (1986) 2555–2560.
- [55] R. Viswanatha, S. Sapra, B. Satpati, P.V. Satyam, B.N. Devb, D.D. Sarma, *J. Mater. Chem.* 14 (2004) 661–668.
- [56] J.W. Lee, S.M. Lee, C.S. Park, G.T. Park, H.E. Kim, *J. Sol–Gel Sci. Technol.* 42 (2007) 305–308.
- [57] D.G. Zhao, S.J. Xu, M.H. Xie, S.Y. Tong, Hui Yang, *Appl. Phys. Lett.* 83 (2003) 677–679.
- [58] G.A.C.M. Spierings, G.J.M. Dormans, W.G.J. Moors, M.J.E. Ulenaers, P.K. Larsen, *J. Appl. Phys.* 78 (1995) 1926–1933.
- [59] C.H. Jiang, S.P. Chen, Z.Y. Xu, *PTCA A: Phys. Test.* 38 (2002) 478–481 (in Chinese).
- [60] M. Zhang, J.W. He, *Ordnance Mater. Sci. Eng.* 24 (2001) 68–71 (in Chinese).
- [61] F.Z. Ren, M.S. Zheng, G.S. Zhou, W.Z. Zhao, H.C. Gu, *Rare Met. Mater. Eng.* 33 (2004) 706–709 (in Chinese).
- [62] B.J. Roman, A.E. Ewald, *Phys. Rev. B* 5 (1972) 3914–3932.
- [63] B.A. Kulp, K.A. Gale, *Phys. Rev.* 156 (1967) 877–880.
- [64] E.A. Meulenkamp, *J. Phys. Chem. B* 102 (1998) 5566–5572.
- [65] E.M. Wong, J.E. Bonevich, P.C. Searson, *J. Phys. Chem. B* 102 (1998) 7770–7775.
- [66] N. Khan, J. Li, *Appl. Phys. Lett.* 89 (2006) 151916.
- [67] R. Meske, E. Schnack, *Mech. Mater.* 35 (2003) 19–34.
- [68] G.R. Zhao, *Piezoelectr. Acoustoopt.* 6 (1983) 60–72, 43 (in Chinese).